ACS APPLIED MATERIALS & INTERFACES

Research Article

www.acsami.org

Carrier Transport at Metal/Amorphous Hafnium–Indium–Zinc Oxide Interfaces

Seoungjun Kim,[†] Youngun Gil,[†] Youngran Choi,[†] Kyoung-Kook Kim,[‡] Hyung Joong Yun,[§] Byoungchul Son,[§,#] Chel-Jong Choi,[†] and Hyunsoo Kim*[,†]

[†]School of Semiconductor and Chemical Engineering, Semiconductor Physics Research Center, Chonbuk National University, Jeonju, Chonbuk 561-756, Korea

[‡]Department of Nano-Optical Engineering, Korea Polytechnic University, Siheung 429-793, Korea

[§]Division of Materials Science, Korea Basic Science Institute, Daejeon 305-333, Korea

[#]Analysis Center for Research Advancement, Korea Advanced Institute of Science and Technology, Daejeon 34141, Korea

Supporting Information

ABSTRACT: In this paper, the carrier transport mechanism at the metal/amorphous hafnium–indium–zinc oxide (a-HIZO) interface was investigated. The contact properties were found to be predominantly affected by the degree of interfacial reaction between the metals and a-HIZO; that is, a higher tendency to form metal oxide phases leads to excellent Ohmic contact via tunneling, which is associated with the generated donor-like oxygen vacancies. In this case, the Schottky–Mott theory is not applicable. Meanwhile, metals that do not form interfacial metal oxide, such as Pd, follow the Schottky–Mott theory, which results in rectifying Schottky behavior. The Schottky characteristics of the Pd contact to a-HIZO can be explained in terms of the barrier inhomogeneity model, which yields a mean barrier height of 1.40 eV and a standard deviation of 0.14 eV. The work function of a-HIZO could therefore be estimated as 3.7 eV, which is in good agreement with the ultraviolet photoelectron spectroscopy (3.68 eV). Our findings will be useful for establishing a strategy to form Ohmic or Schottky contacts to a-HIZO films, which will be essential for fabricating reliable high-performance electronic devices.

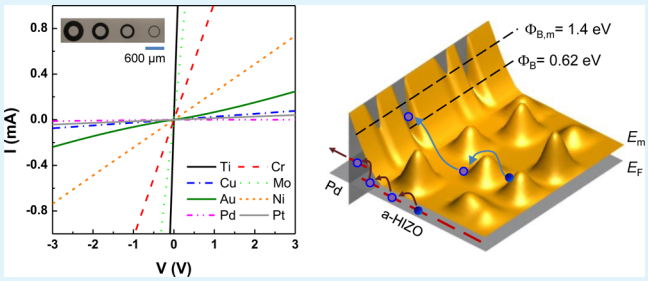

KEYWORDS: *carrier transport, contact, HIZO, Schottky–Mott, Ohmic, Schottky, interfacial reaction*

INTRODUCTION

Zn-based oxide semiconductors such as ZnO, InZnO, ZnSnO, AlZnSnO, GaZnSnO, InZrZnO, and InZnSnO are of great significance for applications in transparent thin-film transistors (TFTs), solar cells, and gas sensors. These semiconductors offer many advantages, including large-scale fabrication feasibility, low cost, usability in low-temperature processes, good transparency associated with large bandgap energies (E_g), and sensitivity to gas molecules.[1−3] In particular, amorphous oxide semiconductors such as GaInZnO (a-GIZO) or HfInZnO (a-HIZO) have been extensively investigated during the past several years because they exhibit excellent electrical properties that satisfy the requirements for use in current display applications.[4−7] These include a high field-effect mobility of ∼10 $cm^2/(V\ s)$, an on–off current ratio of up to $\sim 10^6$, a subthreshold voltage swing of ∼0.25 V/decade, and low-temperature processing feasibility for flexible substrates.

However, the a-GIZO semiconductor, which has been most widely used as representative active channel material in TFT devices, suffers from long-term bias instability associated with disruptions of atomic arrangements; i.e., a generation of donor-like oxygen vacancies caused by the dissociation of GIZO.[8,9] Meanwhile, TFTs fabricated with a-HIZO semiconductors produced improved TFT performance characteristics and better bias-induced stability associated with the nature of Hf atoms.[10−12] Specifically, compared to Ga atoms, Hf atoms have a stronger thermodynamic tendency to form metal oxides, suppressing the dissociation of HIZO and hence impeding the generation of unexpected charge carriers.[13,14] Therefore, numerous attempts have been made to allow a-HIZO semiconductors to replace the current a-GIZO materials in future display applications.

To use a-HIZO semiconductors, it is crucial to understand the carrier transport at metal/a-HIZO interfaces for device fabrications. Indeed, the formation of an Ohmic contact is essentially required for the fabrication of low-resistance and reliable metal–insulator–semiconductor field-effect transistors (MISFETs) because the contact resistance at the source and drain regions has a significant influence on the device performance.[15−19] On one hand, the demonstration of Schottky contact in a-HIZO, which has not been reported yet, would extend its application to metal–semiconductor field-effect

Received: July 10, 2015
Accepted: September 27, 2015
Published: September 27, 2015

DOI: 10.1021/acsami.5b06223
ACS Appl. Mater. Interfaces 2015, 7, 22385−22393

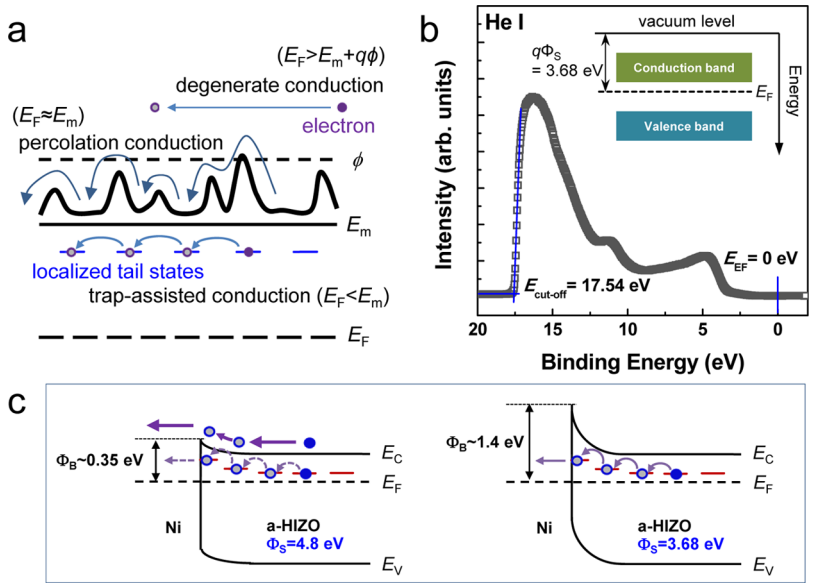

Figure 1. (a) Distinctive electronic energy band diagram of oxide semiconductors, explaining possible carrier transport mechanisms such as trap-assisted conduction, percolation conduction, and degenerate conduction. (b) The UPS spectrum of the a-HIZO sample. (c) The schematic band diagrams of the Ni contact to a-HIZO, which were drawn when Φ_S = 4.8 and 3.68 eV.

transistors (MESFETs), which can produce better device performance with lower operating voltages and enhanced feasible channel mobility. Furthermore, an exact understanding of the carrier transport mechanism at the metal/a-HIZO interface is of particular importance for practical applications of a-HIZO semiconductors. However, very few studies have been conducted on this subject.

In this study, we investigated the contact properties and carrier transport mechanism at the metal/a-HIZO interfaces by employing various metals having different work functions (Φ_m), namely, Ti (4.33), Cr (4.5), Cu (4.51), Mo (4.6), Au (5.1), Pd (5.12), Ni (5.15), and Pt (5.65 eV).[20] The electrical properties of contacts were evaluated using transmission line model (TLM) methods[21] and Schottky diodes, by which the current−voltage-temperature ($I-V-T$) measurement was performed to elucidate the transport mechanism. The carrier transport mechanism was further supported by the measurements of X-ray photoemission spectroscopy (XPS) depth profiling, ultraviolet photoelectron spectroscopy (UPS), an atomic force microscope (AFM), and a Kelvin probe force microscope (KPFM). On the basis of these findings, the carrier transport mechanism at the metal/a-HIZO interface, the work function of a-HIZO semiconductor (Φ_S), and the strategy to form Ohmic or Schottky contacts could be eventually suggested.

EXPERIMENTAL SECTION

In this study, a 70 nm thick a-HIZO film deposited on glass substrates by an RF magnetron sputtering system was used. The sputtering was performed under the following conditions: gas ratio of Ar/O_2 = 10, chamber pressure of 5 mTorr, and RF power of 80 W.[22] The composition of the sputter target was HfO_2:In_2O_3:ZnO = 0.15:1:2 mol %. Hall-effect measurements performed for the five a-HIZO films using the van der Pauw method yielded an average electron carrier concentration (N) of $6.5 \times 10^{16} \pm 3.5 \times 10^{14}$ cm^{-3} and a Hall mobility (μ) of 9.7 ± 0.02 $cm^2/(V\ s)$. Note that, despite the absence of post-thermal annealing, our samples showed good electrical properties in terms of N and μ, which are comparable to the postannealed amorphous semiconductors used for TFT applications. To investigate the structural and electronic properties of a-HIZO surfaces, the AFM and KPFM measurements were performed using a Nanoscope IV multimode AFM system. A scan was performed in the tapping mode to simultaneously obtain the surface morphology and surface potentials at a bias of 1 V. In addition, a UPS measurement was performed with a He I resonance lamp ($h\nu$ = 21.22 eV) to estimate Φ_S.

To investigate the metal contacts on a-HIZO, TLM patterns with circular geometry (diameter of the inner circle was 300 μm and the distances between the inner and outer circles were d = 20, 60, 100, and 150 μm) were defined using a conventional photolithographic technique, as shown in the inset of Figure 2a. As contact metals, 200 nm-thick Ti, Cr, Cu, Au, Pd, Ni, and Pt were then deposited on the patterned a-HIZO samples using an e-beam evaporator, while 200 nm-thick Mo was deposited using a dc sputter instrument. In addition, a Schottky diode was also fabricated using circular active geometry shown in the inset of Figure 5a. For example, Pd (200 nm) and Ti/Au (50 nm/50 nm) were deposited on the central circle with a diameter of 500 μm and the surrounding region to form Schottky and Ohmic contacts, respectively. All electrical characteristics of the contacts were evaluated using a parameter analyzer (HP 4156A) equipped with a vacuum chamber (<2×10^{-2} Torr) and a variable-temperature chuck system. An $I-V-T$ measurement was performed to elucidate the carrier transport mechanism at the contact interface, in the temperature ranges 150−300 K for the TLM and 300−380 K for Schottky diodes. Finally, the interfacial reaction between metals and a-HIZO was investigated using XPS as a function of the etching time; i.e., the metal surface, contact/a-HIZO interface, and the bulk a-HIZO were investigated comparatively.

RESULTS AND DISCUSSION

Prior to investigating the carrier transport mechanism at the metal/a-HIZO interfaces, the transport behavior in bulk a-HIZO semiconductors should be understood. The carrier transport in the oxide semiconductors has been explained by the percolation conduction theory[23] and the small polaronic hopping conduction.[24,25] However, the possibility of polaronic hopping conduction was excluded in our study for several reasons, which are explained in Figure S1 of Supporting Information. According to Adler's percolation conduction model for oxide semiconductors,[23] the carrier transport was influenced by the distinctive electronic energy band diagram of oxide semiconductors. This can be schematically drawn with

DOI: 10.1021/acsami.5b06223
ACS Appl. Mater. Interfaces 2015, 7, 22385−22393

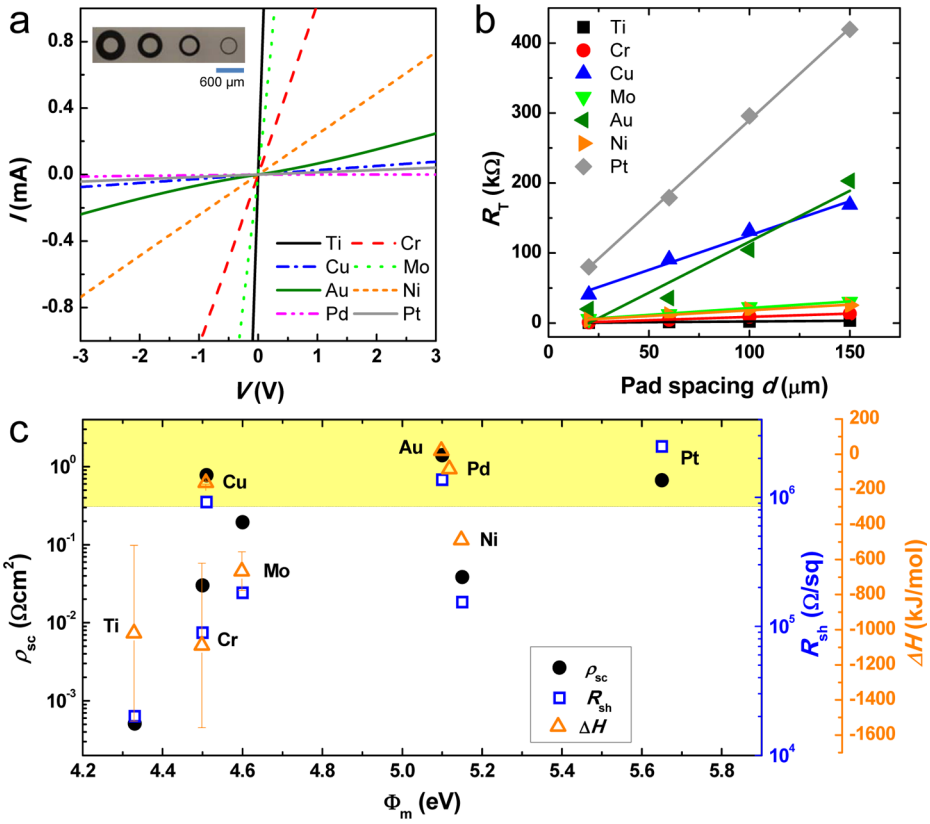

Figure 2. (a) I−V characteristics, (b) R_T−d plots, and (c) the obtained ρ_{sc} and R_{sh} data (plotted along with the ΔH) for the Ti, Cr, Cu, Mo, Au, Ni, Pd, and Pt contacts to a-HIZO.

distributed potential barriers around a mobility edge (E_m) having an average height of ϕ and localized tail-states residing 80−150 meV below E_m (see Figure 1a).[5,6] Specifically, the carrier transport in a-HIZO semiconductors can be classified into three categories, on the basis of the position of the Fermi level (E_F). That is, the carrier transport may occur through multiple trap and release events at the localized tail-states if the E_F resides within the localized tail-states; this is a condition known as the trap-assisted conduction.[26−28] Percolation conduction occurring as a result of released carriers overcoming potential barriers would appear as the predominant conduction mechanism if the value of E_F is close to that of E_m.[27−30] Last, the degenerate conduction will be dominant if E_F exceeds the potential barrier height, i.e., $E_F > E_m + q\phi$.[26−28]

On the basis of the measured N value (6.5×10^{16} cm^{-3}), the position of E_F can be calculated using equation[27,28,31]

$$E_F - E_m = \frac{kT}{q}\ln\left[\frac{N}{N_C} + \frac{1}{2^{3/2}}\left(\frac{N}{N_C}\right)^2\right] \quad (1)$$

where k is the Boltzmann constant, q is the electronic charge, and N_C is the effective density of states. Assuming that the N_C value of a-HIZO is close to that of a-GIZO (5.2×10^{18} cm^{-3}),[5] E_F is found to locate 113 meV below E_m. This indicates that E_F resides near the localized tail-states. Therefore, trap-assisted percolation conduction, in which the carrier transport may occur partly through trap-assisted conduction and partly through percolation conduction, is expected to dominate the carrier transport in the a-HIZO films.

On the basis of the carrier transport behavior in the a-HIZO semiconductor, the carrier transport at the metal/a-HIZO interface would be explained only if the Schottky barrier height (Φ_B) is defined. The Φ_B can be estimated according to the Schottky−Mott theory, i.e.[21]

$$\Phi_B = \Phi_S - \Phi_m \quad (2)$$

where Φ_S is the work function of the a-HIZO semiconductor. Unfortunately, however, little is known about the accuracy of the Φ_S values. For example, Choi et al. assumed the electron affinity of a-HIZO to be 4.1 eV for their simulation of a-HIZO TFTs, i.e., $\Phi_S \approx 4.1$ eV.[32] Recently, Jeon et al. obtained a Φ_S value of 4.8 eV using KPFM measurements,[33] which is much larger than ∼4.1 eV[34] or 4.5 eV[35] (for a-GIZO). A large discrepancy between the reported Φ_S values suggests that the Φ_S of our a-HIZO sample should be further investigated.

Figure 1b shows the UPS spectrum of the a-HIZO sample (obtained under irradiation by He I line photons). On the basis of a cutoff binding energy (E_{cutoff}) value of 17.54 eV and the relation[36,37]

$$\Phi_{a-HIZO} = h\nu - |E_{cut\text{-}off} - E_F| \quad (3)$$

where h is Planck's constant, ν is the frequency of irradiated photons ($h\nu = 21.22$ eV), and $E_F = 0$ eV, a Φ_S value of 3.68 eV can be obtained. Note that the obtained Φ_S value is closer to the value used by Choi et al. (∼4.1 eV), but much lower than that used by Jeon et al. (4.8 eV). This is presumably due to the different surface states, crystallographic features, and atomic composition of a-HIZO samples.

Although further investigations for obtaining the precise Φ_S value of a-HIZO should be carried out, it would be meaningful to predict the carrier transport at the metal/a-HIZO interface for both extreme cases (Φ_S = 3.68 and 4.8 eV), as shown in

DOI: 10.1021/acsami.5b06223
ACS Appl. Mater. Interfaces 2015, 7, 22385−22393

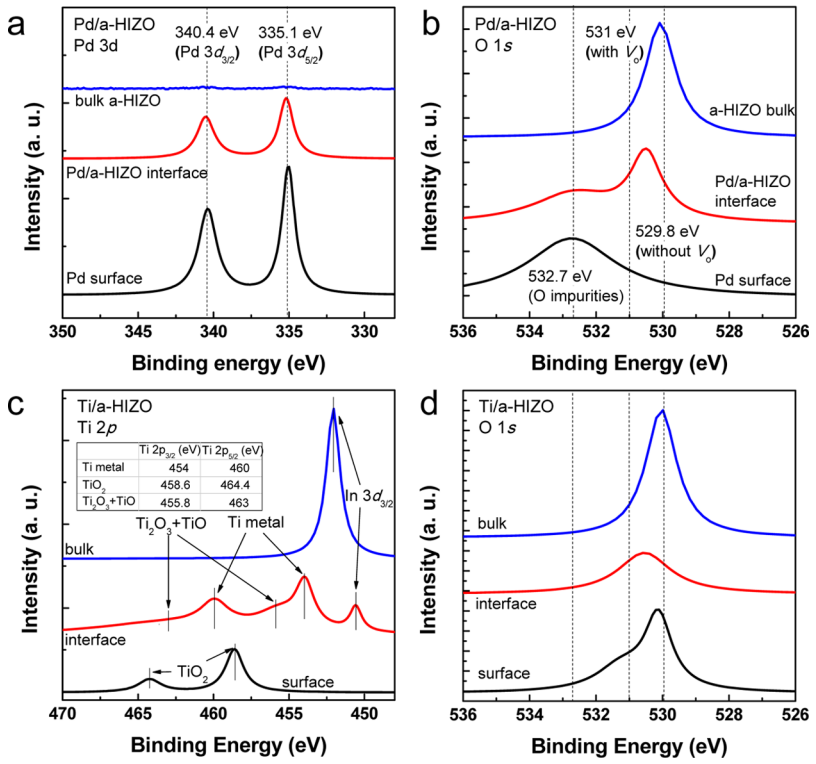

Figure 3. X-ray photoelectron spectroscopy (XPS) spectra of the (a) Pd 3d and (b) O 1s core levels for the Pd/a-HIZO contact, and the (c) Ti 2p and (d) O 1s core levels for the Ti/a-HIZO contact, as obtained at the metal surface, contact interface, and the bulk a-HIZO.

Figure 1c. The schematic band diagram was drawn by assuming that Ni (Φ_m = 5.15 eV) was used as the contact metal. For Φ_S = 4.8 eV, note that a very small Φ_B of 0.35 eV is obtained at the contact interface, indicating that the Ni contact would show very weak rectifying behavior. Meanwhile, metals having $\Phi_m \leq$ 4.8 eV (such as Ti, Cr, Mo, and Cu) are likely to form Ohmic contacts to a-HIZO. Notably, in the case of Φ_S = 3.68 eV, all metals used in this study are likely to show rectifying Schottky behavior; this is particularly true for Pd, Ni, Au, and Pt contacts, because they have the large Φ_B of $\geq \sim$1.4 eV. In this case, trap-assisted percolation conduction is expected to play a key role in carrier transport at the metal/a-HIZO interface, as depicted in Figure 1c, where trap-assisted tunneling and/or percolation conduction through the local shallow barriers can enhance transport.[26−28] Note that, in this connection, all metals may exhibit Ohmic behavior because of the effect of reduced Φ_B.

To investigate practical contact behavior, the electrical properties of contacts were evaluated using TLM methods, as shown in Figure 2. Figure 2a shows the $I-V$ characteristics of the Ti, Cr, Mo, Cu, Au, Pd, Ni, and Pt contacts to a-HIZO, as obtained from adjacent contact pads with d = 20 μm. It is shown that the $I-V$ curves are significantly dependent on the contact metals. For example, Ti exhibited the steepest $I-V$ curve among all contacts, while Pt, Cu, Au, and especially Pd produced poor $I-V$ curves. It is also noteworthy that, although most contacts exhibited linear $I-V$ curves, the slopes of the $I-V$ curves were quite different depending on the metals used. This indicates that either the specific contact resistances (ρ_{sc}) or the sheet resistance of a-HIZO (R_{sh}) is affected by the contact metals. The linear regression fit of the total resistances (R_T) versus d data yields both ρ_{sc} and R_{sh} values according to[21]

$$R_T = \frac{R_{sh}}{2\pi L}(d + 2L_T)C \quad (4)$$

where L is the radius of the inner circle, L_T is the transfer length, and C is the correction factor (see Figure 2b). Here, L_T and C are given by $L_T = (\rho_{sc}/R_{sh})^{1/2}$ and $C = L/d \ln(1 + d/L)$, respectively.

Figure 2c summarizes the obtained ρ_{sc} and R_{sh} values as a function of Φ_m. For the Pd contact, both ρ_{sc} and R_{sh} values could not be obtained due to the unavailability of a TLM theory model; i.e., no meaningful linear regression relationship was observed in the R_T versus d plots. Note that the samples show minimal Φ_m dependence, indicating that the Schottky−Mott theory is not appropriate for explaining the carrier transport at the contact interface. More noticeably, both ρ_{sc} and R_{sh} values showed nearly the same contact-metal dependence; i.e., the higher the ρ_{sc}, the larger the R_{sh}, and vice versa. Indeed, these findings are quite interesting, considering that the electrical conductivity of the a-HIZO layer was significantly influenced by the contact metals as well as contact resistance.

Very recently, while investigating the contact properties of Ti and Ag on a-GIZO, Choi et al.[35] showed that the Ohmic contact was determined by the degree of interfacial reaction between the metal and a-GIZO. For example, owing to a higher tendency to form interfacial Ti oxide, Ti produced excellent Ohmic contact to a-GIZO, where the generated oxygen vacancies (acting as donors) could reduce the R_{sh} value of the a-GIZO layer and enhance the Ohmic contact via tunneling. Meanwhile, Ag produced a relatively poor Ohmic contact, owing to the much less favorable generation of interfacial Ag oxides. To investigate if this model is valid in our samples, the standard molar enthalpy of formation at 298.15 K, averaged for all possible metal oxide phases (ΔH: a measure of the thermodynamic tendency to form interfacial metal oxides),[38] was also plotted along with the ρ_{sc} and R_{sh} values, as shown in Figure 2c. Note that both ρ_{sc} and R_{sh} values are in good

DOI: 10.1021/acsami.5b06223
ACS Appl. Mater. Interfaces 2015, 7, 22385−22393

agreement with the ΔH values, indicating that the carrier transport at the metal/a-HIZO interface is dominated by either the degree of interfacial reaction or the degree of generated oxygen vacancies.

It is important to keep in mind that the Pd contact was very poor. According to our hypothesis, this can be attributed partly to the absence of an interfacial Pd oxide phase and partly to the large Φ_B at the Pd/a-HIZO interface. To support this argument, XPS depth profiling was performed for both Pd and Ti contacts, as shown in Figure 3. Figure 3a shows the Pd 3d spectra obtained from the Pd surface, Pd/a-HIZO interface, and a-HIZO bulk region. At the Pd surface, metallic Pd double peaks were observed at binding energies of 335.1 and 340.4 eV, corresponding to Pd $3d_{5/2}$ and Pd $3d_{3/2}$, respectively.[39] Notably, at the same binding energies, metallic Pd double peaks were also definitively observed at the Pd/a-HIZO interface, indicating that no interfacial reaction occurred. Consistently, as shown in Figure 3b, the O 1s spectrum of the Pd surface also showed solely chemisorbed oxygen impurities, such as O^{2-}, O^-, O_2^-, O_2^{2-}, and OH^- ions, at a binding energy of 532.7 eV;[40−42] however, it showed no evidence of the formation of Pd oxide phases. At the interface and bulk regions, the O 1s peaks appeared at approximately 529−531 eV, which originate from the oxygen in amorphous oxide lattices without (529.8 eV) and with (531.0 eV) oxygen vacancies.[40] Indeed, the absence of a Pd oxide phase can be predicted thermodynamically by comparing the ΔH values of each oxide phase; i.e., ΔH_{PdO} (−85 kJ/mol) ≪ ΔH_{HfO} (−1144.7 kJ/mol), ΔH_{In2O3} (−925.8 kJ/mol), ΔH_{ZnO} (−350.5 kJ/mol).[38]

In contrast, the Ti 2p spectra showed a remarkable oxidation at the Ti surface, as confirmed by TiO_2 peaks at 458.6 (Ti $2p_{3/2}$) and 464.4 eV (Ti $2p_{5/2}$), but showed minimal oxygen impurities chemisorbed on the Ti surface (see Figure 3c). In addition, inspection of the Ti/a-HIZO interface revealed the presence of multiple phases comprising Ti_2O_3 (455.8), TiO (463), metallic Ti (454 and 460 eV), and metallic In,[43] indicating that significant interfacial oxidation had occurred. Consistently, Ti oxides were observed at the Ti surface and contact interface, as observed in the O 1s spectra (Figure 3d). Indeed, the formation of an interfacial oxide is due to the significantly large ΔH value of Ti oxide phases, e.g., Ti_2O_3 (−1520.9 kJ/mol) and TiO (−519 kJ/mol),[38] leading to an out-diffusion of oxygen atoms from the a-HIZO layer and hence generating oxygen vacancies near the contact. Therefore, the Ohmic contact can be easily obtained via tunneling or field emission (FE).

To investigate if the contact is dominated by tunneling transport, $I-V-T$ measurements were performed for the Ti/a-HIZO sample, as shown in Figure 4a. Note that the $I-V$ curve remained nearly unchanged (slightly improved) upon increasing T, which is a typical feature of tunneling.[21] Accordingly, the obtained ρ_{sc} value was also nearly constant as a function of T, as shown in Figure 4b. According to the contact theory,[21] the theoretical ρ_{sc} value can be estimated on the basis of the appropriate conduction model, which can be determined depending on the T and the tunneling parameter (E_{00}); i.e., thermionic emission (TE) dominates when $E_{00}/kT < 0.5$, thermionic field emission (TFE) dominates when $0.5 < E_{00}/kT < 5$, and FE dominates when $E_{00}/kT > 5$. Here, E_{00} is given by $E_{00} = (qh/4\pi)(N/\varepsilon_s m^*)^{1/2}$, where m^* is the electron effective mass ($m^* = 0.35m_e$) and ε_s is the dielectric constant of a-HIZO.[44] With $N = 6.5 \times 10^{16}$ cm^{-3} and $T = 300$ K, the

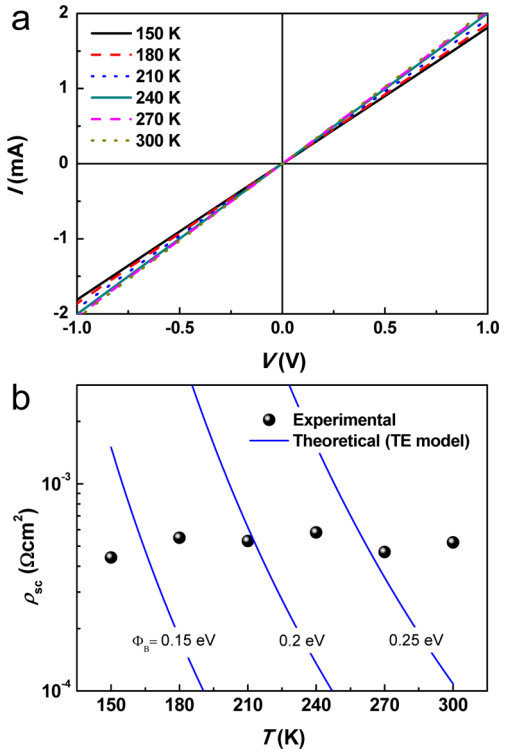

Figure 4. (a) $I-V-T$ characteristics and (b) $\rho_{sc}-T$ plots of the Ti contact to a-HIZO.

calculation shows that E_{00}/kT is as low as 0.09, which lies in the TE regime, namely[21]

$$\rho_{sc} = \frac{k}{qA^{**}T}\exp\left(\frac{q\Phi_B}{kT}\right) \quad (5)$$

where A^{**} is the Richardson constant (42 A cm^{-2} K^{-2}). Here, A^{**} was calculated using the following equation: $A^{**} = 4\pi qm^*k^2/h^3 = 120m^*/m_e$.[44] Note that the experimental ρ_{sc} significantly deviates from the value obtained from TE theory, indicating that the pure TE model cannot explain the carrier transport at the contact. Meanwhile, the insensitive temperature dependence of the ρ_{sc} value can be explained in terms of tunneling associated with the generated interfacial oxygen vacancies.

For metals exhibiting Ohmic behavior, the generation of oxygen vacancies near the a-HIZO surface occurring as a result of an interfacial reaction between the metal and a-HIZO was suggested as the primary Ohmic mechanism, which caused tunneling. However, it should also be noted that the formation of the interfacial oxide layer had a negative impact on carrier transport. Specifically, in the presence of an interfacial oxide layer with thickness δ, the Φ_B can be increased as follows:[45,46]

$$q\Phi_B = q\Phi_{B0} + \frac{2kT}{\hbar}\sqrt{2m^*\chi}\,\delta \quad (6)$$

Here Φ_{B0} is the Schottky barrier height in the absence of the interfacial oxide, $\hbar = h/2\pi$, and χ is the mean tunneling barrier for carrier injection from the metal to semiconductor. A rough calculation shows that ~10 Å-thick oxide layers can increase the barrier height by 0.1−0.2 eV. However, the Ti contact showed the best Ohmic behavior with a significantly reduced R_{sh} value. Moreover, the $I-V-T$ measurements showed typical tunneling behavior, indicating that the large number of donor-like oxygen

DOI: 10.1021/acsami.5b06223
ACS Appl. Mater. Interfaces 2015, 7, 22385−22393

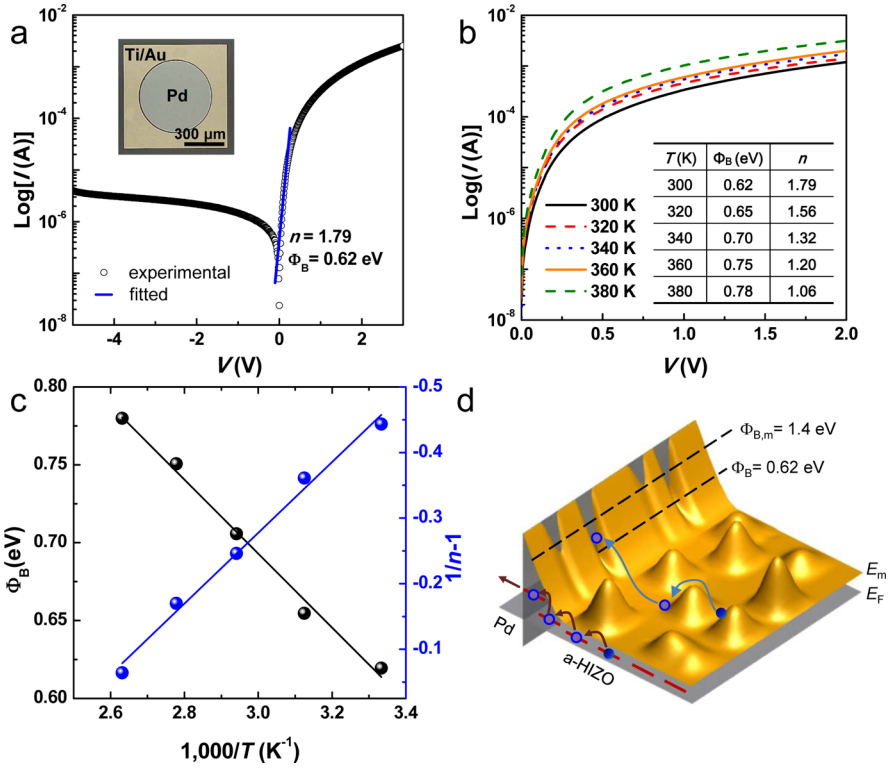

Figure 5. (a) $I-V$ characteristics of the Pd/a-HIZO Schottky diode, analyzed using the TE model. The inset shows a top-view optical microscopy image of the fabricated diodes. (b) $I-V-T$ characteristics of the Pd/a-HIZO Schottky diode. The inset shows the obtained Φ_B and n values as a function of T. (c) Reciprocal temperature dependence of Φ_B and $1/n - 1$. (d) Schematic band diagram of Pd contact to a-HIZO, exhibiting the possible carrier transport through the local shallow barriers or trap-assisted tunneling.

vacancies has a much greater influence on carrier transport at the Ti/a-HIZO contact than the increased Φ_B.

It is particularly important to investigate whether the Schottky diode can be obtained using Pd metal. It will also be feasible to estimate the Φ_B if Pd Schottky diodes are successfully fabricated, giving valuable information with respect to the Φ_S. In this sense, the Schottky diodes were fabricated using the Pd Schottky contact and Ti/Au Ohmic contact, as shown in the inset of Figure 5a. Figure 5a shows the semilogarithmic $I-V$ curve of the Pd/a-HIZO Schottky diode obtained at 300 K. Interestingly, rectifying behavior was observed, as expected. To analyze the $I-V$ characteristics of the Pd Schottky diode, in principle, the TE model should be used because of the low N value (note that there are no donor-like oxygen vacancies at the Pd/a-HIZO interface); i.e., the forward $I-V$ curve from the TE model is given by[21]

$$I = AA^{**}T^2 \exp\left(-\frac{q\Phi_B}{kT}\right)\left[\exp\left(\frac{qV}{nkT}\right) - 1\right] \tag{7}$$

where A is the area of Schottky contact and n is the ideality factor. The theoretical fits of the forward $I-V$ curves using eq 7 revealed that n = 1.79 and Φ_B = 0.62 eV. According to the Schottky–Mott theory discussed earlier, Φ_B was expected to be 0.32 eV when Φ_S = 4.8 eV,[33] and 1.42 eV when Φ_S = 3.68 eV (UPS results). However, the obtained Φ_B of 0.62 eV was somewhat different from both expected Φ_B values. Furthermore, the obtained n value was much larger than unity,[21] indicating that nonideal carrier transport occurred at the contact interface; thus, the pure TE model may not be suitable to explain the carrier transport.

Previously, carrier transport at the Schottky contact to a-GIZO could be explained in terms of the barrier inhomogeneity model,[29,47] in which it can be assumed that the barrier heights follow a Gaussian distribution with a mean value of $\Phi_{B,m}$ and a standard deviation of σ, i.e.[48,49]

$$\Phi_B(T) = \Phi_{B,m}(T = 0) - \frac{q\sigma^2}{2kT} \tag{8}$$

The distinctive feature of the barrier inhomogeneity model is the positive temperature dependence with respect to Φ_B, as predicted in eq 8; i.e., the higher the value of T, the larger the obtained Φ_B. Specifically, carriers with low thermal energy can flow through the local shallow barrier at relatively low temperatures, resulting in a reduced mean barrier height. As the temperature increases, a large fraction of carriers with higher thermal energy tends to flow through larger barriers because the local shallow barriers with relatively small cross sections are occupied. To investigate whether the barrier inhomogeneity model is applicable to the Pd/a-HIZO sample, $I-V-T$ measurements were performed in the 300–380 K temperature range, as shown in Figure 5b. In this figure, note that $I-V$ characteristics are significantly dependent on T and V. Accordingly, the Φ_B and n values were found to depend significantly on T, as shown in the inset of Figure 5b.

Figure 5c shows the reciprocal temperature dependence of both Φ_B and $1/n - 1$. According to the TE theory, Φ_B and n should remain constant as a function of temperature.[21] However, Φ_B increased monotonically with increasing temperature, leading to a straight-line relationship in the Φ_B versus $1/T$ plots, which is consistent with eq 8. This indicates that the barrier inhomogeneity model can reasonably explain the carrier

DOI: 10.1021/acsami.5b06223
ACS Appl. Mater. Interfaces 2015, 7, 22385–22393

transport at the Pd/a-HIZO interface. From a linear fit using eq 8, the $\Phi_{B,m}$ at 0 K and σ were found to be 1.40 and 0.14 eV, respectively. Note that the obtained $\Phi_{B,m}$ value is in excellent agreement with the theoretical Φ_B of 1.42 eV, which was predicted on the basis of the Schottky−Mott theory under the assumption that Φ_S = 3.68 eV. This indicates that the work function of a-HIZO is closer to our measured value of 3.68 eV, rather than the reported values of ~4.1[32] or 4.8 eV.[33] However, the definitive work function for a-HIZO remains to be elucidated.

The reason for the underestimation of Φ_S might be associated with the surface charging effect,[50] hydrocarbon contamination,[51] and different atomic compositions.[52] The surface charging effect, which modulates the vacuum level of a-HIZO, is known to be more pronounced in the insulators,[50] while our sample is a semiconductor. Therefore, the surface charging effect seems relatively insignificant in our case. Furthermore, Φ_S varies with the hydrocarbon contaminants incorporated from the atmosphere. However, this possibility also seems minor because, prior to UPS measurement, the a-HIZO sample was presputtered with Ar plasma to produce a clean surface. Therefore, the large deviation can be primarily ascribed to the different atomic compositions of a-HIZO. Specifically, note that the target composition of a-HIZO exhibiting Φ_S = 4.8 eV was HfO_2:In_2O_3:ZnO = 0.07:0.525:0.403 at. %,[33] while the composition of our sample (Φ_S = 3.68 eV) was HfO_2:In_2O_3:ZnO = 0.15:1:2 mol %. Consequently, the deposited a-HIZO film also showed a very different atomic composition[33] (see Supporting Information Figure S2). Furthermore, the thickness (70 nm) of our a-HIZO was greater than that from the previous work (20 nm).[33] Generally, the atomic composition or structure is also known to change with thickness.[52] That is, owing to different growth conditions and atomic compositions, the different atomic arrangement or structure is expected to cause a deviation in Φ_S.

In Figure 5c, the bias voltage dependence of Φ_B can be explained on the basis of the temperature dependence of the n value according to[53,54]

$$\frac{1}{n} - 1 = -\rho_a + \frac{q\rho_b}{2kT} \tag{9}$$

where ρ_a and ρ_b are the voltage coefficients used in the following relationships: $\Phi_{B,m} = \Phi_{B0,m} + \rho_a V$ and $\sigma^2 = \sigma^2_0 + \rho_b V$, where the subscript "0" refers to the zero bias case. On the basis of the barrier inhomogeneity model, ρ_a and ρ_b should also be temperature independent, resulting in a straight line in the $1/n - 1$ versus T^{-1} plots, as shown in Figure 5c. The linear regression fit of the experimental data using eq 9 yielded ρ_a = −1.34 and ρ_b = −93 mV, indicating that both $\Phi_{B,m}$ and n have negative forward bias dependences. As reported previously, the negative signs of both voltage coefficients imply that the bias voltage homogenizes the potential fluctuation, i.e., the higher the bias, the narrower the barrier distribution.[53]

The practical origin of local shallow barriers that cause large barrier height fluctuations (or large σ values) should be addressed. According to the literature,[4−6,26,29] the carrier transport in bulk oxide semiconductors was reported to be influenced by percolation hopping conduction over the distributed potential barriers around the conduction band edge, as described in Figure 1. Nomura and Hosono et al.[4−6] suggested that the randomly distributed Ga^{3+} and Zn^{2+} ions in a-GIZO may result in the distribution of potential barriers around the conduction band edge. For example, these randomly distributed ions, which constitute the intrinsic nature of amorphous structures, modulate the electronic structure around the conduction band edge and may form statistical potential distributions at the contact interface. In addition, the disorder-induced localized tail-states near the band edge may act as the pathway for carrier transport at the contact interfaces.[28] Consequently, carrier transport at the Pd/a-HIZO interface can be explained by combining these two possibilities as shown in Figure 5d, in which the carrier can flow through the localized tail-states and/or shallow potential barriers in order to move into the metal at relatively low temperatures. In Figure 5d, it is noteworthy that the Φ_B of 0.62 eV obtained from the TE model is comparable to the energy level of the local shallow barriers (with the lowest barrier height), while the $\Phi_{B,m}$ of 1.40 eV reflects the actual barrier height that most carriers have to overcome.

The evidence for the large fluctuation of potential barriers could be obtained from AFM and KPFM, as shown in Figure 6.

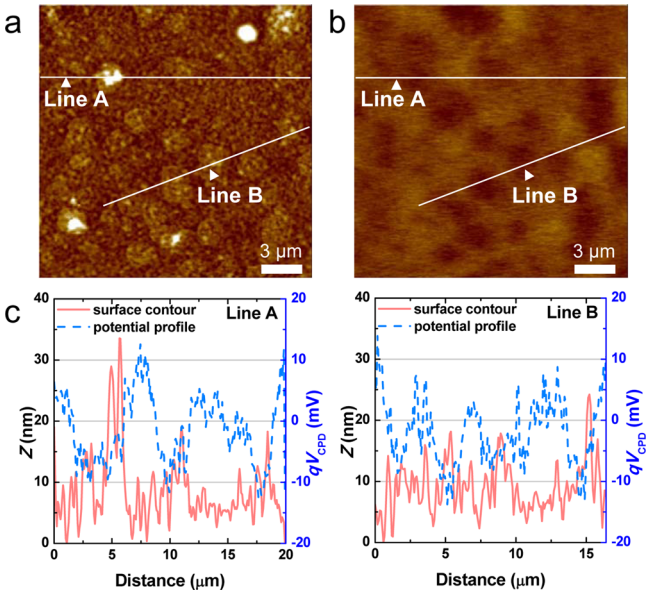

Figure 6. (a) Surface morphology and (b) corresponding surface potential (V_{CPD}) mapping images obtained over the same 20 × 20 μm^2 a-HIZO sample area. (c) The surface contour and potential profiles of lines A and B.

Figure 6a,b shows the surface morphology and corresponding surface potential images obtained over the same 20 × 20 μm^2 a-HIZO sample area. According to KPFM theory, the contact potential difference (V_{CPD}) between the conducting AFM tip and the a-HIZO surface can be obtained using the relation[55]

$$V_{CPD} = \frac{\Phi_{tip} - \Phi_S}{-q} \tag{10}$$

where Φ_{tip} is the work function of the Pt-coated tip (5.65 eV). Therefore, it should be noted that the V_{CPD} mapping data represent Φ_S fluctuation on the a-HIZO surface. Note that, although the observed surface undulations in AFM images are somewhat in agreement with the KPFM results, the morphological line profiles denoted as lines A and B in AFM images do not match the V_{CPD} line profiles, as shown in Figure 6c. This indicates that the surface roughness has little correlation with the fluctuations of potential barriers. Meanwhile, V_{CPD} fluctuations with an average variation range of ~24

DOI: 10.1021/acsami.5b06223
ACS Appl. Mater. Interfaces 2015, 7, 22385−22393

meV were found to be uniformly distributed over the entire area. This indicates that the presence of local shallow barriers can affect the contact properties significantly, because a number of local shallow barriers can exist within the contact area.

Lastly, it would be meaningful to compare the contact behavior of wide bandgap amorphous semiconductors with typical single-crystal GaN semiconductors. The Schottky–Mott theory is applicable to GaN semiconductors;[56] i.e., the contact properties have a significant Φ_m dependence. Therefore, Ohmic contacts or Schottky diodes could be fabricated on GaN semiconductors by selecting a metal with the proper Φ_m. However, for amorphous semiconductors, the Schottky–Mott theory was less significant than it was for GaN due to the interfacial oxidation reaction between metals and amorphous semiconductors; i.e., the higher the tendency to form interfacial metal oxides, the better the obtained Ohmic contact. Consequently, the formation of Schottky diodes was very limited, since only unreactive metals with large Φ_m should be employed.

CONCLUSION

The fundamental carrier transport mechanisms at metal/a-HIZO interfaces were investigated. The metals, including Ti, Cr, Mo, and Ni, produced a good Ohmic contact to a-HIZO without regard to their work functions, indicating that the Schottky–Mott theory cannot explain the carrier transport. Meanwhile, Pd, Cu, Au, and Pt yielded poor Ohmic or Schottky contacts. Analysis using XPS and thermodynamic considerations showed that the carrier transport at the metal/a-HIZO interface was predominantly affected by the degree of interfacial oxidation; i.e., a higher tendency to form metal oxides will increase the occurrence of carrier transport due to tunneling. Meanwhile, an effective Schottky diode could be created by employing a Pd contact, owing to its insignificant interfacial reaction and its large work function. The carrier transport at the Pd/a-HIZO interface could be reasonably explained in terms of the barrier inhomogeneity model, providing valuable information with respect to the mean barrier height (1.4 ± 0.14 eV) at the Pd/a-HIZO interface and the work function of a-HIZO (~3.7 eV), as estimated by the Schottky–Mott theory and UPS results.

ASSOCIATED CONTENT

Supporting Information

The Supporting Information is available free of charge on the ACS Publications website at DOI: 10.1021/acsami.5b06223.

Figures detailing carrier transport and depth profiles (PDF)

AUTHOR INFORMATION

Corresponding Author

*E-mail: hskim7@jbnu.ac.kr. Phone: +82 63 270 3974. Fax: +82 63 270 3585.

Author Contributions

S.K. and Y.G. contributed equally to this work.

Notes

The authors declare no competing financial interest.

ACKNOWLEDGMENTS

This research was supported in part by Basic Science Research Program through the National Research Foundation of Korea (NRF) funded by the Ministry of Education, Science and Technology (2014R1A1A1A05007455, 2015R1A6A1A04020421) and in part by the Transfer Machine Specialized Lighting Core Technology Development Professional Manpower Training Project (Project NO: N0001363) funded by the Ministry of Trade, Industry & Energy (MOTIE, Korea).

REFERENCES

(1) Nomura, K.; Ohta, H.; Ueda, K.; Kamiya, T.; Hirano, M.; Hosono, H. Thin-Film Transistor Fabricated in Single-Crystalline Transparent Oxide Semiconductor. *Science* **2003**, *300*, 1269–1272.

(2) Ozgur, U.; Alivov, Y. I.; Liu, C.; Teke, A.; Reshchikov, M. A.; Dogan, S.; Avrutin, V.; Cho, S. J.; Morkoc, H. A Comprehensive Review of ZnO Materials and Devices. *J. Appl. Phys.* **2005**, *98*, 041301.

(3) *Transparent Conductive Zinc Oxide: Basics and Applications in Solar Cells*, 1st ed.; Ellmer, K., Klein, A., Bernd, R., Eds.; Springer: Heidelberg, Germany, 2008.

(4) Nomura, K.; Ohta, H.; Takagi, A.; Kamiya, T.; Hirano, M.; Hosono, H. Room-Temperature Fabrication of Transparent Flexible Thin-Film Transistors Using Amorphous Oxide Semiconductors. *Nature* **2004**, *432*, 488–492.

(5) Kamiya, T.; Nomura, K.; Hosono, H. Origins of High Mobility and Low Operation Voltage of Amorphous Oxide TFTs: Electronic Structure, Electron Transport, Defects and Doping. *J. Disp. Technol.* **2009**, *5*, 273–288.

(6) Kamiya, T.; Hosono, H. Material Characteristics and Applications of Transparent Amorphous Oxide Semiconductors. *NPG Asia Mater.* **2010**, *2*, 15–22.

(7) Kim, C. J.; Kim, S.; Lee, J. H.; Park, J. S.; Kim, S.; Park, J.; Lee, E.; Lee, J.; Park, Y.; Kim, J. H.; Shin, S. T.; Chung, U. I. Amorphous Hafnium-Indium-Zinc Oxide Semiconductor Thin Film Transistors. *Appl. Phys. Lett.* **2009**, *95*, 252103.

(8) Park, J. S.; Kim, K.; Park, Y. G.; Mo, Y. G.; Kim, H. D.; Jeong, J. K. Novel ZrInZnO Thin-Film Transistor with Excellent Stability. *Adv. Mater.* **2009**, *21*, 329–333.

(9) Kamiya, T. Present Status of Amorphous InGaZnO Thin-Film Transistors. *Sci. Technol. Adv. Mater.* **2010**, *11*, 044305.

(10) Chong, E.; Jo, K. C.; Lee, S. Y. High Stability of Amorphous Hafnium–Indium–Zinc-Oxide Thin Film Transistor. *Appl. Phys. Lett.* **2010**, *96*, 152102.

(11) Park, J. C.; Kim, S.; Kim, S.; Kim, C.; Song, I.; Park, Y.; Jung, U. I.; Kim, D. H.; Lee, J. S. Highly Stable Transparent Amorphous Oxide Semiconductor Thin-Film Transistors Having Double-Stacked Active Layers. *Adv. Mater.* **2010**, *22*, 5512–5516.

(12) Kim, H. S.; Park, J. S.; Jeong, H. K.; Son, K. S.; Kim, T. S.; Seon, J. B.; Lee, E.; Chung, J. G.; Kim, D. H.; Ryu, M.; Lee, S. Y. Density of States-Based Design of Metal Oxide Thin-Film Transistors for High Mobility and Superior Photostability. *ACS Appl. Mater. Interfaces* **2012**, *4*, 5416–5421.

(13) Jeong, W. H.; Kim, G. H.; Shin, H. S.; Du Ahn, B.; Kim, H. J.; Ryu, M.-K.; Park, K.-B.; Seon, J.-B.; Lee, S. Y. Investigating Addition Effect of Hafnium in InZnO Thin Film Transistors Using a Solution Process. *Appl. Phys. Lett.* **2010**, *96*, 093503.

(14) Jeong, W. H.; Kim, G. H.; Kim, D. L.; Shin, H. S.; Kim, H. J.; Ryu, M.-K.; Park, K.-B.; Seon, J.-B.; Lee, S.-Y. Effects of Hf Incorporation in Solution-Processed Hf-InZnO TFTs. *Thin Solid Films* **2011**, *519*, 5740–5743.

(15) Shimura, Y.; Nomura, K.; Yanagi, H.; Kamiya, T.; Hirano, M.; Hosono, H. Specific Contact Resistances between Amorphous Oxide Semiconductor In–Ga–Zn-O and Metallic Electrodes. *Thin Solid Films* **2008**, *516*, 5899–5902.

(16) Park, J.; Kim, C.; Kim, S.; Song, I.; Kim, S.; Kang, D.; Lim, H.; Yin, H.; Jung, R.; Lee, E.; Lee, J.; Kwon, K.-W.; Park, Y. Source/Drain Series-Resistance Effects in Amorphous Gallium-Indium Zinc-Oxide Thin Film Transistors. *IEEE Electron Device Lett.* **2008**, *29*, 879–881.

(17) Barquinha, P.; Vilá, A. M.; Gonçalves, G.; Pereira, L.; Martins, R.; Morante, J. R.; Fortunato, E. Gallium–Indium–Zinc-Oxide-Based

DOI: 10.1021/acsami.5b06223
ACS Appl. Mater. Interfaces 2015, 7, 22385–22393

Thin-Film Transistors: Influence of the Source/Drain Material. *IEEE Trans. Electron Devices* **2008**, *55*, 954−960.
(18) Lee, J. E.; Sharma, B. K.; Lee, S.-K.; Jeon, H.; Hong, B. H.; Lee, H.-J.; Ahn, J.-H. Thermal Stability of Metal Ohmic Contacts in Indium Gallium Zinc Oxide Transistors Using a Graphene Barrier Layer. *Appl. Phys. Lett.* **2013**, *102*, 113112.
(19) Luo, D.; Xu, H.; Zhao, M.; Li, M.; Xu, M.; Zou, J.; Tao, H.; Wang, L.; Peng, J. Influence of Source and Drain Contacts on the Properties of Indium-Gallium-Zinc-Oxide Thin-Film Transistors based on Amorphous Carbon Nanofilm as Barrier Layer. *ACS Appl. Mater. Interfaces* **2015**, *7*, 3633−3640.
(20) Hałas, S. 100 years of work function. *Mater. Sci.-Poland* **2006**, *24*, 951−968.
(21) Schroder, D. K. *Semiconductor Material and Device Characterization*, 3rd ed.; John Wiley & Sons: Hoboken, NJ, 2006.
(22) Kim, S.; Gil, Y.; Kim, K.-K.; Ahn, K.-S.; Kim, H. Carrier Transport Mechanism of Mo Contact to Amorphous Hafnium Indium Zinc Oxides. *Phys. Status Solidi A* **2014**, *211*, 1818−1821.
(23) Adler, D.; Flora, L. P.; Senturia, S. D. Electrical Conductivity in Disordered Systems. *Solid State Commun.* **1973**, *12*, 9−12.
(24) Zhao, B.; Kaspar, T. C.; Droubay, T. C.; McCloy, J.; Bowden, M. E.; Shutthanandan, V.; Heald, S. M.; Chambers, S. A. Electrical Transport Properties of Ti-Doped Fe_2O_3 (0001) Epitaxial Films. *Phys. Rev. B: Condens. Matter Mater. Phys.* **2011**, *84*, 245325.
(25) Chatman, S.; Pearce, C. I.; Rosso, K. M. Charge Transport at Ti-Doped Hematite (001)/Aqueous Interfaces. *Chem. Mater.* **2015**, *27*, 1665−1673.
(26) Lee, C.; Cobb, B.; Dodabalapur, A. Band Transport and Mobility Edge in Amorphous Solution-Processed Zinc Tin Oxide Thin-Film Transistors. *Appl. Phys. Lett.* **2010**, *97*, 203505.
(27) Lee, S.; Ghaffarzadeh, K.; Nathan, A.; Robertson, J.; Jeon, S.; Kim, C.; Song, I.-H.; Chung, U.-I. Trap-Limited and Percolation Conduction Mechanisms in Amorphous Oxide Semiconductor Thin Film Transistors. *Appl. Phys. Lett.* **2011**, *98*, 203508.
(28) Kim, S.; Kim, K.-K.; Kim, H. Carrier Transport Mechanism at Metal/amorphous Gallium Indium Zinc Oxides interfaces. *Appl. Phys. Lett.* **2012**, *101*, 033506.
(29) Kim, H.; Kim, K.-K.; Lee, S.-N.; Ryou, J.-H.; Dupuis, R. D. Low Resistance Ti/Au Contacts to Amorphous Gallium Indium Zinc Oxides. *Appl. Phys. Lett.* **2011**, *98*, 112107.
(30) Kirkpatrick, S. Percolation and Conduction. *Rev. Mod. Phys.* **1973**, *45*, 574−588.
(31) Joyce, W. B.; Dixon, R. W. Analytic Approximations for the Fermi Energy of an Ideal Fermi Gas. *Appl. Phys. Lett.* **1977**, *31*, 354−356.
(32) Kim, S. J.; Lee, S. Y.; Lee, Y. W.; Lee, W. G.; Yoon, K. S.; Kwon, J. Y.; Han, M. K. Effect of Channel Layer Thickness on Characteristics and Stability of Amorphous Hafnium-Indium-Zinc Oxide Thin Film Transistors. *Jpn. J. Appl. Phys.* **2011**, *50*, 024104.
(33) Jeon, S.; Song, I.; Lee, S.; Ryu, B.; Ahn, S.-E.; Lee, E.; Kim, Y.; Nathan, A.; Robertson, J.; Chung, U.-I. Origin of High Photoconductive Gain in Fully Transparent Heterojunction Nanocrystalline Oxide Image Sensors and Interconnects. *Adv. Mater.* **2014**, *26*, 7102−7109.
(34) Barquinha, P.; Vilá, A.; Gonçalves, G.; Pereira, L.; Martins, R.; Morante, J.; Fortunato, E. The Role of Source and Drain Material in the Performance of GIZO Based Thin-Film Transistors. *Phys. Status Solidi A* **2008**, *205*, 1905−1909.
(35) Choi, K.-H.; Kim, H.-K. Correlation between Ti Source/Drain Contact and Performance of InGaZnO based Thin Film Transistors. *Appl. Phys. Lett.* **2013**, *102*, 052103.
(36) Klein, A.; Körber, C.; Wachau, A.; Saüberlich, F.; Gassenbauer, Y.; Harvey, S. P.; Proffit, D. E.; Mason, T. O. Transparent Conducting Oxides for Photovoltaics: Manipulation of Fermi Level, Work Function and Energy Band Alignment. *Materials* **2010**, *3*, 4892−4914.
(37) Liu, T.; Zhang, X.; Zhang, J.; Wang, W.; Feng, L.; Wu, L.; Li, W.; Zeng, G.; Li, B. Interface Study of ITO/ZnO and ITO/SnO_2 Complex Transparent Conductive Layers and Their Effect on CdTe Solar Cells. *Int. J. Photoenergy* **2013**, *2013*, 765938.
(38) Haynes, W. M. *CRC Handbook of Chemistry and Physics*, 92nd ed.; CRC Press: New York, 2011.
(39) Yang, S.; Dong, J.; Yao, Z.; Shen, C.; Shi, X.; Tian, Y.; Lin, S.; Zhang, X. One-Pot Synthesis of Graphene-Supported Monodisperse Pd Nanoparticles as Catalyst for Formic Acid Electro-oxidation. *Sci. Rep.* **2014**, *4*, 4501.
(40) Yang, S.-H.; Kim, J. Y.; Park, M. J.; Choi, K.-H.; Kwak, J. S.; Kim, H.-K.; Lee, J.-M. Low Resistance Ohmic Contacts to Amorphous IGZO Thin Films by Hydrogen Plasma Treatment. *Surf. Coat. Technol.* **2012**, *206*, 5067−5071.
(41) Studenikin, S. A.; Golego, N.; Cocivera, M. Carrier Mobility and Density Contributions to Photoconductivity Transients in Polycrystalline ZnO Films. *J. Appl. Phys.* **2000**, *87*, 2413−2421.
(42) Henrich, V. E.; Cox, P. A. *The Surface Science of Metal Oxides*; Cambridge University Press: New York, 1994.
(43) Chrcanovic, B. R.; Pedrosa, A. R.; Martins, M. D. Chemical and Topographic Analysis of Treated Surfaces of Five Different Commercial Dental Titanium Implants. *Mater. Res.* **2012**, *15*, 372−382.
(44) Denny, Y. R.; Shin, H. C.; Seo, S.; Oh, S. K.; Kang, H. J.; Tahir, D.; Heo, S.; Chung, J. G.; Lee, J. C.; Tougaard, S. Electronic and Optical Properties of Hafnium Indium Zinc Oxide Thin Film by XPS and REELS. *J. Electron Spectrosc. Relat. Phenom.* **2012**, *185*, 18−22.
(45) Hattori, K.; Izumi, Y. The Electrical Characteristics of Degenerate InP Schottky Diodes with an Interfacial Layer. *J. Appl. Phys.* **1982**, *53*, 6906−6910.
(46) Jung, S.; Song, K.-R.; Lee, S.-N.; Kim, H. Wet Chemical Etching of Semipolar GaN Planes to Brighter and Cost-Competitive Light Emitters. *Adv. Mater.* **2013**, *25*, 4470−4476.
(47) Kim, H.; Kim, S.; Kim, K.-K.; Lee, S.-N.; Ahn, K.-S. Electrical Characteristics of Pt Schottky Contacts Fabricated on Amorphous Gallium Indium Zinc Oxides. *Jpn. J. Appl. Phys.* **2011**, *50*, 105702.
(48) Padovani, F. A.; Stratton, R. Field and Thermionic-Field Emission in Schottky Barriers. *Solid-State Electron.* **1966**, *9*, 695−707.
(49) Rhoderick, E. H. Metal-Semiconductor Contacts. *IEE Proc., Part I: Solid-State Electron Devices* **1982**, *129*, 1−14.
(50) Ko, C.; Yang, Z.; Ramanathan, S. Work Function of Vanadium Dioxide Thin Films Across the Metal-Insulator Transition and the Role of Surface Nonstiochiometry. *ACS Appl. Mater. Interfaces* **2011**, *3*, 3396−3401.
(51) Whitcher, T. J.; Yeoh, K. H.; Chua, C. L.; Woon, K. L.; Chanlek, N.; Nakajima, H.; Saisopa, T.; Songsiriritthigul, P. The Effect of Carbon Contamination and Argon Ion Sputtering on the Work Function of Chlorinated Indium Tin Oxide. *Curr. Appl. Phys.* **2014**, *14*, 472−475.
(52) Luan, H.; Alshareef, H. N.; Harris, H. R.; Wen, H. C.; Choi, K.; Senzaki, Y.; Majhi, P.; Lee, B.-H. Evaluation of Titanium Silicon Nitride as Gate Electrodes for Complementary Metal-Oxide Semiconductor. *Appl. Phys. Lett.* **2006**, *88*, 142113.
(53) Werner, J. H.; Güttler, H. H. Barrier Inhomogeneities at Schottky Contacts. *J. Appl. Phys.* **1991**, *69*, 1522−1533.
(54) Tung, R. T. Electron Transport at Metal-Semiconductor Interfaces: General Theory. *Phys. Rev. B: Condens. Matter Mater. Phys.* **1992**, *45*, 13509−13523.
(55) Melitz, W.; Shen, J.; Kummel, A. C.; Lee, S. Kelvin Probe Force Microscopy and Its Application. *Surf. Sci. Rep.* **2011**, *66*, 1−27.
(56) Schmitz, A.; Ping, A.; Khan, M.; Chen, Q.; Yang, J.; Adesida, I. Metal Contacts to n-type GaN. *J. Electron. Mater.* **1998**, *27*, 255−260.

DOI: 10.1021/acsami.5b06223
ACS Appl. Mater. Interfaces 2015, 7, 22385−22393